

PCCP

Accepted Manuscript



This is an *Accepted Manuscript*, which has been through the Royal Society of Chemistry peer review process and has been accepted for publication.

Accepted Manuscripts are published online shortly after acceptance, before technical editing, formatting and proof reading. Using this free service, authors can make their results available to the community, in citable form, before we publish the edited article. We will replace this *Accepted Manuscript* with the edited and formatted *Advance Article* as soon as it is available.

You can find more information about *Accepted Manuscripts* in the [Information for Authors](#).

Please note that technical editing may introduce minor changes to the text and/or graphics, which may alter content. The journal's standard [Terms & Conditions](#) and the [Ethical guidelines](#) still apply. In no event shall the Royal Society of Chemistry be held responsible for any errors or omissions in this *Accepted Manuscript* or any consequences arising from the use of any information it contains.

Quantum Size Effects on the Optical Properties of nc-Si QDs Embedded in a-SiO_x Matrix Synthesized by Spontaneous Plasma Processing

Debajyoti Das* and Arup Samanta¹

Nano-Science Group, Energy Research Unit,
Indian Association for the Cultivation of Science,
Jadavpur, Kolkata-700 032, India

Abstract:

Quantum confinement effects on optical transitions in ensembles of nc-Si QDs in a-SiO_x matrix has been evident by simultaneously considering the dielectric function dispersions obtained by optical modeling with spectroscopic ellipsometry, the absorption edge, and the photoluminescence peak. Diminution of the peak amplitude in the ϵ_2 -spectra for reducing diameter of nc-Si QDs could arise due to the disappearance of excitonic effects in the E₁ transition, while the peak broadening indicate an amplification of disorder in Si QDs. Energy blue shift happens to take place in an analogous fashion for all the characteristic parameters, on decreasing size of the nc-Si QDs for diameters in the range 6.5 < d < 2.0 nm. The band gap widening with the reduction of QD size is well supported by the first-principles calculations based on quantum confinement, while studies on the Stokes shift in the optical gap from the PL data could comprehend on the imperfect passivation of the surface defects on tiny nc-Si QDs. Low dimensional nc-Si QDs (~2 nm in diameter) assembled in large density (~2.3 × 10¹² cm⁻²) embedded in a-SiO_x matrix synthesized by spontaneous and low-temperature (300°C) RF plasma processing, compatible to CMOS technology, is highly conducive for device applications. Systematic changes in composition and characteristics, including the thickness, of the individual sub-layers of the nc-Si QD thin films can be comprehensively pursued through a nondestructive process by ellipsometric simulation which could, thereby, enormously contribute in the precise optimization of the deposition parameters suitable for specific device fabrication e.g., all-silicon tandem solar cells and light emitting diodes, using silicon nanotechnology.

Keywords: nc-Si quantum dots, ellipsometry, optical modeling, wide band gap, quantum size effect.

* Author to whom all correspondence should be addressed,
E-mail: erdd@iacs.res.in (D. Das); Fax: +91(33)24732805.

¹ Present address: Research Institute of Electronics, Shizuoka University,
3-5-1 Johoku, Naka-ku, Hamamatsu 432-8011, Japan

1. Introduction:

In recent years, nanocrystalline silicon quantum dots (nc-Si QDs) embedded in SiO_x matrix have been widely studied for its use as the charge storage medium in non-volatile memory devices,¹ in Si-based light emitting diodes (LED's) for applications in optoelectronic devices,² single electron devices,³ with the advantage of being compatible with the mainstream complementary metal oxide semiconductor (CMOS) process and in all-silicon tandem solar cells.⁴ The key issue in creating such structures is that the size, position, and density of the nc-Si QDs have to be precisely controlled. One of the significantly promising techniques to form such nc-Si QDs structures within SiO_x matrix is the spontaneous plasma processing of He-diluted ($\text{SiH}_4 + \text{CO}_2$) gas mixture even at a low substrate temperature of 300°C , compatible for device fabrication.^{5,6} While efficient photoluminescence (PL)^{4,5,7,8} and electroluminescence (EL)^{9,10,11,12} in nc-Si QDs embedded in a- SiO_x matrix have demonstrated enormous device feasibility of the material including multi-colour light emitting devices^{13,14}, it still remains necessary to accurately determine its dielectric functions and optical constants, in addition to the compositional and thickness characteristics of its different sub-layers, in order to perform reliable device modeling.

In addition to theoretical calculations,^{15,16,17} a number of reports are available on experimental studies on the dielectric properties of nanocrystalline silicon quantum dots once embedded in a dielectric medium, in particular. Recently, some simulation process based on fitting of the spectroscopic ellipsometry (SE) data have been reported, involving various models e.g., Lorentz oscillator (LO) model,¹⁸ Forouhi-Bloomer (FB) model,^{19,20} Tauc-Lorentz-oscillator (TLO)^{21,22} model, etc. The BEMA model has been successfully employed to evaluate the structural composition characteristics of different sublayer configuration of nano-crystalline silicon thin films grown from H_2 -diluted SiH_4 plasma in Hot-wire CVD, Ar-assisted SiH_4 plasma and Ar-assisted H_2 -diluted SiH_4 plasma in RF-PECVD.^{23,24} On the other hand, the TL model has been satisfactorily utilized in determining the size varying changes in the optical properties of Si-ncs embedded in SiO_x matrix, considering the Si:O compositional characteristic of the dielectric matrix remaining unchanged.^{25,26} For thin film system where Si-ncs are embedded in amorphous SiC dielectric matrix, the chemical composition of which changes on sample to sample leading to consistent changes in the optical property of the amorphous component, the BEMA model accompanied by TL model for amorphous part has been successfully applied for each layer.²⁷



The present work deals with a comprehensive study on nc-Si QDs embedded in a-SiO_x matrix, by optical simulation of the ellipsometry data in the photon-energy range ~1.5–6.0 eV. The optical modeling of the complex system consisting of nc-Si QDs and the a-SiO_x matrix has been done with the combination of Bruggmann effective medium (BEMA) approximation^{28,29,30} and Tauc-Lorentz oscillator (TLO) model³¹ to find out the changes in the compositional characteristics of the ensemble and various optical constants of the nc-Si QDs, in particular, which have been found to be strongly dependent on its size. In addition, a large widening of the optical gap with the reduction in the size of nc-Si QDs has been evaluated and correlated to the predictions of the quantum confinement theory. The spectroscopic ellipsometry analysis has been supported by high-resolution transmission electron microscopy (HRTEM) in determining the size, density and the distribution of the nc-Si QDs, Raman spectroscopy in estimating the crystalline volume fraction in the ensemble and photoluminescence measurements in evaluating the widening of optical gap and its Stokes shift, deviating from the quantum confined assessment. Ensuing analytical techniques and specific spectroscopic simulations could assist in precise optimization of thickness, composition and characteristics of individual sub-layer of the nc-Si QD in a-SiO_x matrix thin film, and facilitate in efficient utilization of the material in the fabrication of devices.

2. Experimental Details:

The nc-Si QDs embedded in a-SiO_x matrix was synthesized on Corning® Eagle2000™ glass substrates and on carbon coated Cu microscope grids (Pacific Grid-Tech, USA), in an indigenously developed PECVD reactor operating at 13.56 MHz. Films were grown from (SiH₄ + CO₂ + He) gas mixture at a fixed flow of SiH₄ (1 SCCM), He (69 SCCM) and maintaining a very low CO₂ flow of 0.08 SCCM, at a low substrate temperature (300°C). Size, density and distribution of the Si-QDs in the films were controlled by varying the RF power from 140 to 220 W in the plasma.

Microstructural properties of the deposited films were investigated by high resolution transmission electron microscope (HRTEM) (JEOL JSM2010) studies on samples ~40 nm thick and deposited on carbon coated copper microscope grids. Raman measurements were performed

at room temperature in a backscattering geometry, using a 488 nm air-cooled Ar⁺ laser as an excitation source. The Raman spectra were obtained using a TRIAX 550 single monochromator with a charge coupled device as the detector. The room temperature photoluminescence measurement was performed using a He–Cd laser as the excitation source operating at 325 nm with an output power of 45 mW.

Optical properties of the nc-Si QDs embedded in a-SiO_x matrix were measured by a fixed angle of incidence spectroscopic ellipsometer (JobinYvon). Let us recall that ellipsometry is an optical method which measures, as a function of the photon energy, the complex reflectance ratio ρ :

$$\rho = \frac{r_p}{r_s} = \tan\Psi e^{i\Delta} \quad (1)$$

where r_p and r_s are the reflection coefficients for a linearly polarized light with its polarization parallel and perpendicular to the incident plane and where Δ and Ψ are the two ellipsometry angles. The experimental ellipsometry angles Ψ and Δ are converted to the pseudo-dielectric function $\langle \varepsilon \rangle$, for a single interface, using:³²

$$\langle \varepsilon \rangle = \sin^2\Phi \left[1 + \left(\frac{1-\rho}{1+\rho} \right)^2 \tan^2\Phi \right] \quad (2)$$

where Φ is the incident angle. The pseudo-dielectric function $\langle \varepsilon \rangle$ characterizes the whole system comprised of air, film and the substrate that reflects the light and it reduces to the dielectric function ε of the material when the reflecting sample has an infinite thickness and a smooth surface.

3. Spectroscopic Ellipsometry Analysis Method:

In the SE analysis, the ellipsometric angles Ψ and Δ can be expressed as functions of the optical constants of the nc-Si QDs, although these functions cannot be displayed with analytical formulas due to their complexity. Based on these functions, a spectral fitting to the experimental data can yield the dielectric function and optical constants of the nc-Si QDs at various photon energies. In the spectral fitting, an appropriate optical dispersion model should be used to



describe the spectral dependence of dielectric functions and the optical constants of the nc-Si QDs. The dielectric functions of the nc-Si QDs and a-SiO_x are modeled by Tauc-Lorentz-oscillator (TLO) and Cauchy models, respectively. Kramers–Kronig consistent TLO model has been used for spectral fitting to parameterize the dielectric functions of nc-Si QDs.^{21,22} The imaginary part (ϵ_2) of the dielectric functions in the TLO model³¹ has been accounted as the product of the Tauc joint density of states with a Lorentz oscillator

$$\epsilon_2(E) = \begin{cases} 0 & \text{for } E \leq E_g \\ \frac{1}{E} \frac{AE_0B(E-E_g)^2}{(E^2-E_0^2)^2+B^2E^2} & \text{for } E > E_g \end{cases} \quad (3)$$

where A is the amplitude of Lorentz oscillator, E_0 is the peak transition energy, E_g is the band gap energy, and B is the broadening factor. The real part (ϵ_1) of the dielectric function is then deduced by Kramers-Kronig integration of ϵ_2 as:

$$\epsilon_1(E) = \epsilon_1(\infty) + \frac{2}{\pi} P \int_{E_g}^{\infty} \frac{\xi \epsilon_2(\xi)}{\xi^2 - E^2} d\xi \quad (4)$$

where P stands for the Cauchy principal part of the integral and $\epsilon_1(\infty)$ stands for the magnitude of ϵ_1 at the infinity.

As mentioned in our earlier work, the nc-Si quantum dots embedded in the a-SiO_x matrix on the glass substrate can be considered with a three-layer structure comprised of: i) thin incubation layer immediately on the substrate surface, ii) bulk nanocrystalline layer with variable composition of amorphous, nanocrystalline, and void components and iii) thin layer representing surface roughness, possessing high void fraction.^{23,33} Therefore, a five-phase model (substrate/incubation layer/bulk layer/surface layers/air) was used in the analysis. Each sublayer can be optically schematized as an effective medium consisting of a-SiO_x, the nc-Si QDs and voids; and its complex dielectric function can be calculated with an appropriate Bruggmann effective medium approximation (BEMA) as

$$f_{\text{nc-Si QDs}} \frac{\epsilon_{\text{nc-Si QDs}}(E) - \epsilon_{\text{eff}}}{\epsilon_{\text{nc-Si QDs}} - 2\epsilon_{\text{eff}}} + f_{\text{a-SiO}_x} \frac{\epsilon_{\text{a-SiO}_x}(E) - \epsilon_{\text{eff}}}{\epsilon_{\text{a-SiO}_x} - 2\epsilon_{\text{eff}}} + f_{\text{voids}} \frac{\epsilon_{\text{voids}}(E) - \epsilon_{\text{eff}}}{\epsilon_{\text{voids}} - 2\epsilon_{\text{eff}}} = 0 \quad (5)$$

where $f_{\text{nc-Si QDs}}$, $f_{\text{a-SiO}_x}$ and f_{voids} are the volume fraction of nc-Si QDs, a-SiO_x and voids, respectively; $\epsilon_{\text{nc-Si QDs}}$, $\epsilon_{\text{a-SiO}_x}$, ϵ_{voids} and ϵ_{eff} are the dielectric function of nc-Si QDs, a-SiO_x, voids and the effective medium, respectively.



The spectral fitting is carried out by freely varying the parameters of the models to minimize the following mean square error (MSE):

$$\text{MSE } (\chi^2) = \frac{1}{2N-M} \sum_{i=1}^N \left[\frac{\Psi_i^{\text{Cal}} - \Psi_i^{\text{Exp}}}{\sigma_{\Psi_i^{\text{Exp}}}} + \frac{\Delta_i^{\text{Cal}} - \Delta_i^{\text{Exp}}}{\sigma_{\Delta_i^{\text{Exp}}}} \right] \quad (6)$$

where N is the number of data points in the spectra, M is the number of variable parameters in the model, χ^2 is the standard deviation on the experimental data points, Ψ^{Exp} and Δ^{Exp} are the measured values of the Ψ and Δ , while Ψ^{Cal} and Δ^{Cal} are the corresponding calculated values, respectively.³²

4. Results:

Transmission electron microscope (TEM) has been used to investigate the detail microstructural properties of the deposited films. Figure 1 represents the bright-field TEM images of samples prepared at different RF powers, demonstrating the QDs as deep dark spots distributed over the network. The HRTEM images presented at the inset of each section show the crystalline planes within corresponding QDs and the associated histograms represent the size



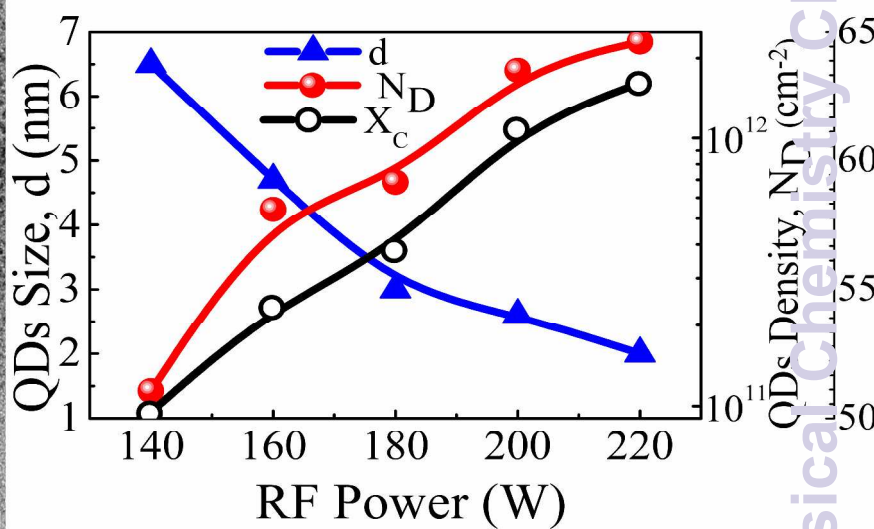
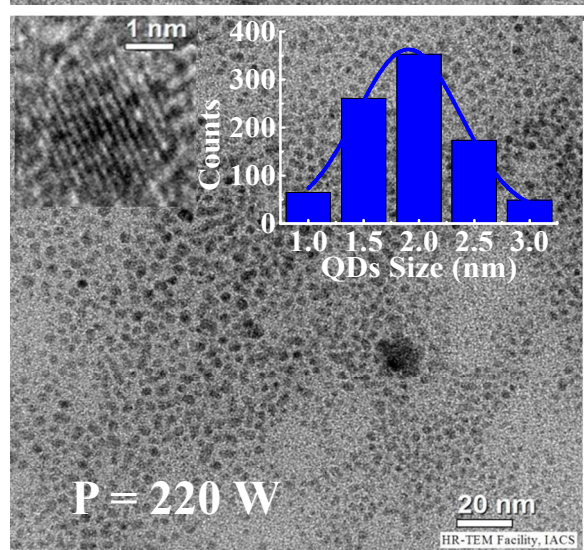
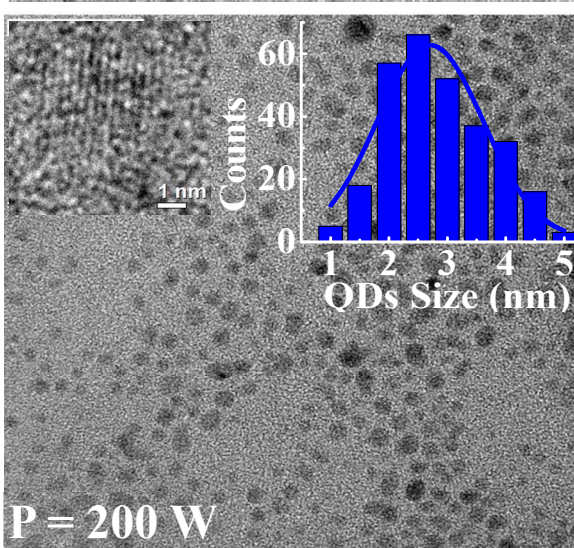
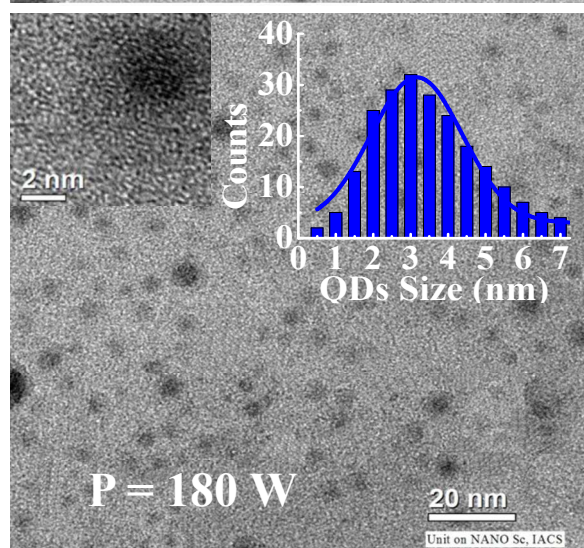
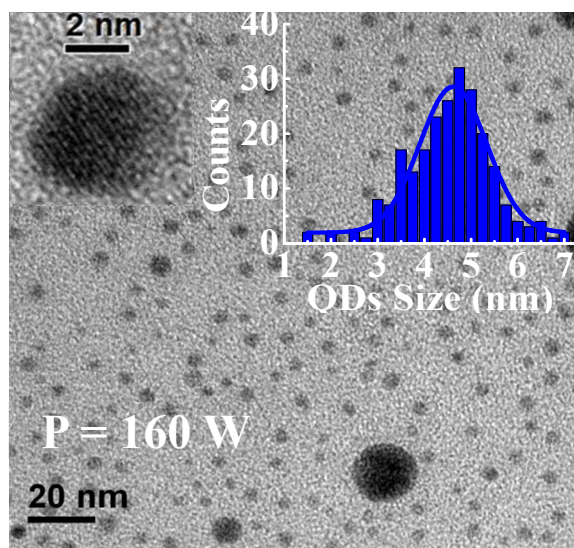
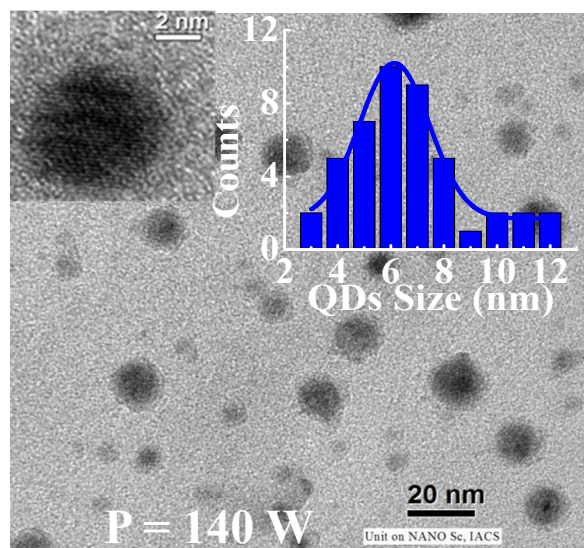


Figure 1. TEM micrograph of nc-Si QDs and the corresponding histogram, demonstrating their size distribution. The HRTEM images at the inset show the crystalline planes within each series of QDs. Graphical presentation on the variation of size and density of the QDs measured from TEM and the variation of Raman crystallinity with RF power applied to the plasma.

distribution of the Si-QDs. In these histogram plots the relatively large size dots have been excluded because of their presence in extremely small numbers. The variations of the size, density and distribution of the QDs with varying the RF power in the plasma have been presented graphically. The average size of the quantum dots reduces gradually from 6.5 nm to 2 nm as the RF power varies from 140 to 220 W, while the density of QDs varies in a reverse manner. Among the present set of samples, the lowest average size of QDs measured from the TEM micrographs is ~ 2 nm with corresponding FWHM of ~ 1 nm and the highest density of $\sim 2.3 \times 10^{12}$ cm $^{-2}$. The volume fraction of crystallinity (X_C) has been estimated from the Raman studies for samples prepared at various RF powers, using typical spectroscopic analysis for nanocrystalline silicon films demonstrated in our earlier reports.^{27,29} Figure 1 exhibits a nature of variation of the crystalline volume fraction similar to the nature of change in number density of the nc-Si QDs, while the former changes in a linear scale and the later in a logarithmic scale. Eventually it signifies that with the systematic increase in the applied RF power the crystallinity improves and most importantly, that contributes to nc-Si QDs of rapidly increasing number density but of gradually reduced dimension, which has significant impact in device application using silicon nanotechnology.



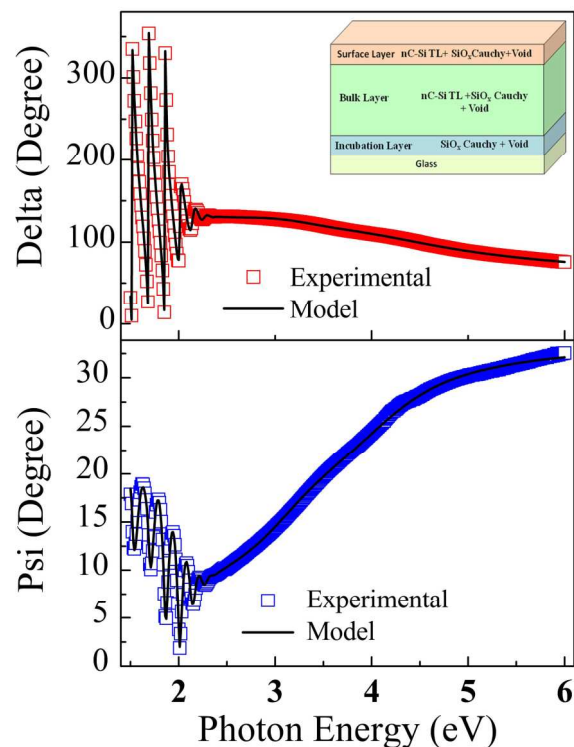


Figure 2. Combination of TLO and BEMA optical modeling of the ellipsometry data, exhibiting good match with the experimentally obtained data points.

In view of the above-mentioned accomplishment in obtaining nc-Si QDs of gradually reduced dimension, $\sim 6.5 - 2$ nm, with simultaneously enhanced number density, $1 \times 10^{11} - 2 \times 10^{12} \text{ cm}^{-2}$, from plasma processing at low substrate temperature conducive to device fabrication, detail understanding of the material's inherent optical and dielectric characteristics appears essential for its efficient utilization in device modeling. Figure 2 shows the experimentally obtained Δ and Ψ spectra of one of the typical samples prepared at $P = 220$ W and the simulated data obtained from the combination of TLO and BEMA optical modeling, based on the methodology described in the above section, that identifies an excellent spectral fitting over a wide energy range from 1.5 to 6.0 eV. The inset presents the modeling scheme applied to individual sub-layers of the thin film system. The detail ellipsometry fitting results, including the thickness of the different layers and their individual composition for all of the five samples have been presented in Table-I. The significantly small MSE (χ^2) ($0.4 < \chi^2 < 0.8$) values ascertain the accuracy of the optical models employed and the goodness of fitting.

Table-I

Details of individual layer-thickness and percentage composition of different sublayers, obtained from fitting of ellipsometry data with the combination of TLO and BEMA optical model.



RF Power (W)	Incubation Thickness (Å)	Incubation Voids (%)	Bulk Thickness (Å)	Bulk Cryst (%)	Bulk Voids (%)	Surface Thickness (Å)	Surface Cryst (%)	Surface Voids (%)	χ^2
140	180.4	26.7	6100.6	49.1	18.2	257.1	34.4	29.2	0.69
160	148.2	21.6	5840.5	52.3	15.6	171.2	40.7	25.3	0.72
180	107.1	20.4	5544.6	57.7	12.8	146.5	44.1	22.7	0.47
200	87.9	17.7	6200.4	61.8	10.5	114.5	48.9	18.6	0.78
220	65.8	14.1	5205.7	68.5	4.6	104.7	52.3	15.4	0.44

The dielectric functions (ϵ_1 and ϵ_2) and optical constants (n and k) of the nc-Si QDs with various average sizes embedded in a-SiO_x matrix, as extracted from the fitting of the ellipsometry data have been presented in Fig. 3 and Fig. 4, respectively. Similar functions and constants of bulk crystalline silicon and amorphous silicon are also included in those figures for comparison. It has been evident from Fig. 3 and Fig. 4 that the nc-Si QDs exhibit a significant suppression in the dielectric functions and optical constants with respect to bulk C-Si, and features a broadened peak structure analogous to that of a-Si.

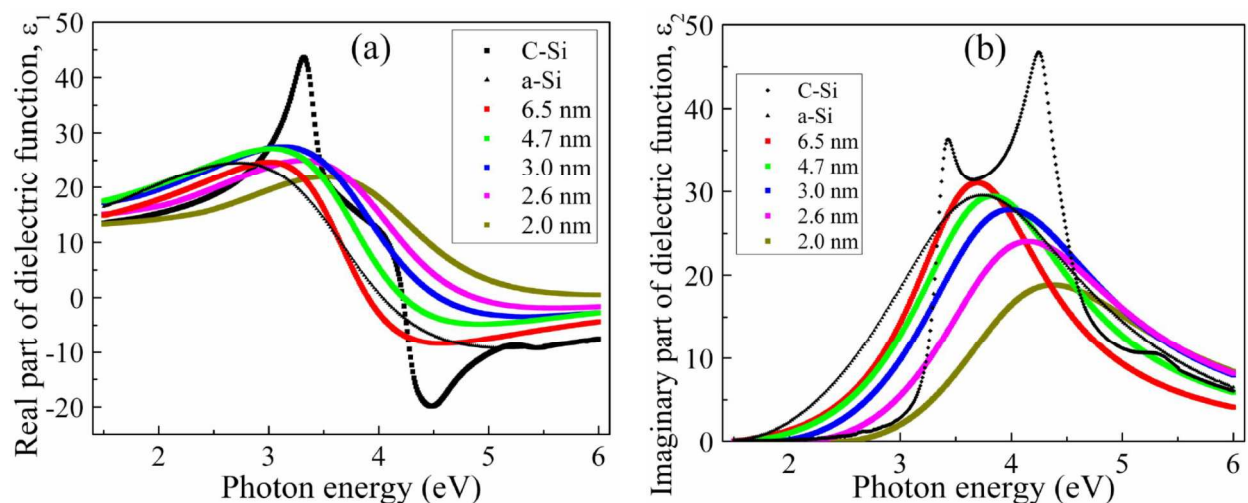


Figure 3. (a) Real (ϵ_1) and (b) imaginary (ϵ_2) parts of the size dependent complex dielectric function of the nc-Si QDs, obtained from the spectral fittings. The dielectric functions of bulk crystalline and amorphous silicon are also included for comparison.

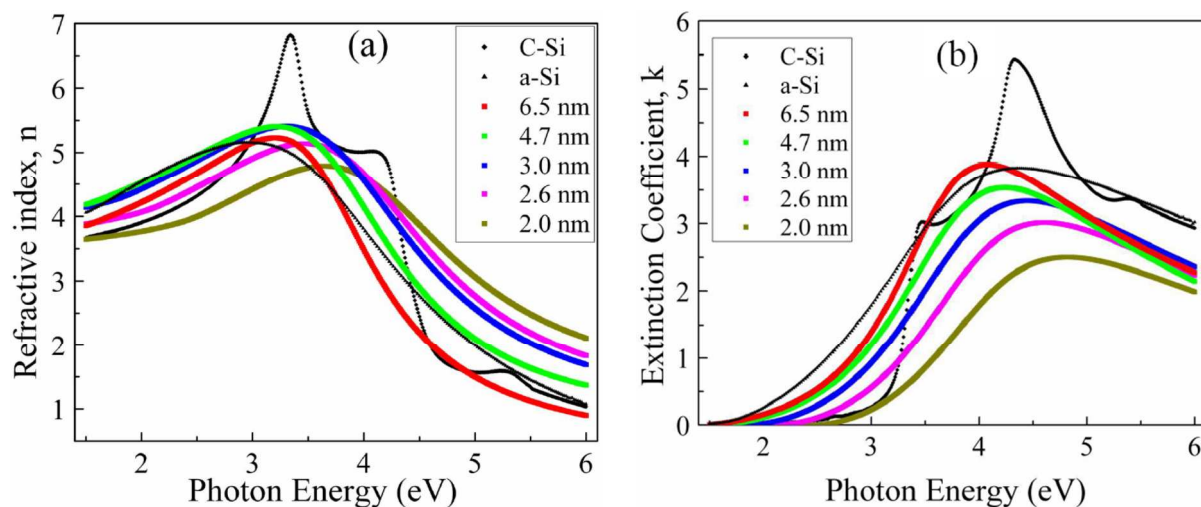


Figure 4. (a) Refractive index (n) and (b) extinction coefficient (k) spectra of the nc-Si QDs of varying average sizes. The optical constants of bulk crystalline and amorphous silicon are also included for comparison.

All the TLO model parameters including A , B , E_0 , E_g and $\epsilon_1(\infty)$ obtained from the simulation of the ellipsometry data are presented in Table-II. For comparison, the corresponding parameters obtained from the literature are also included in the Table-II. The TL parameters are in close agreement with those reported in Ref.22; however, a relatively high value of the parameter A and E_g compared to Ref.21 could be due to the higher density of the size-controlled nc-Si quantum dots accommodated in the matrix for the present set of samples.

Table - II

TLO parameters (A, B, E_0 , $\epsilon_1(\alpha)$ and E_g) extracted from simulation of the ellipsometry data and E_g (PL) estimated from PL data, for various sizes of nc-Si QDs.

RF Power (W)	QD-Size d (nm)	Oscillator Amplitude A	Peak Transition Energy E_0 (eV)	Broadening Parameter B	Offset $\epsilon_1(\alpha)$	Optical Gap E_g (eV)	PL-Gap E_g (PL) (eV)
220	2.0	231.84	4.14	2.18	5.33	2.41	2.24
200	2.6	212.76	4.01	2.07	4.83	2.09	1.95
180	3.0	200.79	3.89	2.06	4.72	1.82	1.73
160	4.7	158.98	3.62	1.82	4.64	1.52	1.46
140	6.5	120.00	3.68	1.52	4.23	1.37	1.35
So et.al. (Ref.22)	3.0	167	4.13	2.03	–	1.87	–
Cen et.al. (Ref.21)	2–3	123	4.35	2.25	–	1.50	–

The nc-Si QDs exhibit a significant increase in the band gap (E_g) with the reduction in the size of QDs compared to that of bulk C-Si, as shown in Table-II. The band gap values of the nc-Si QDs, obtained from the TLO fit, increases from 1.37 to 2.41 eV as the average size of QDs reduced from 6.5 to 2 nm. The band-gap expansion for the nc-Si QDs is consistent with the blue shift of the $(\alpha h\nu)^{1/2}$ vs $h\nu$ plot, as shown in Fig. 5, where $\alpha = 4\pi k/\lambda$ is the absorption coeffi-

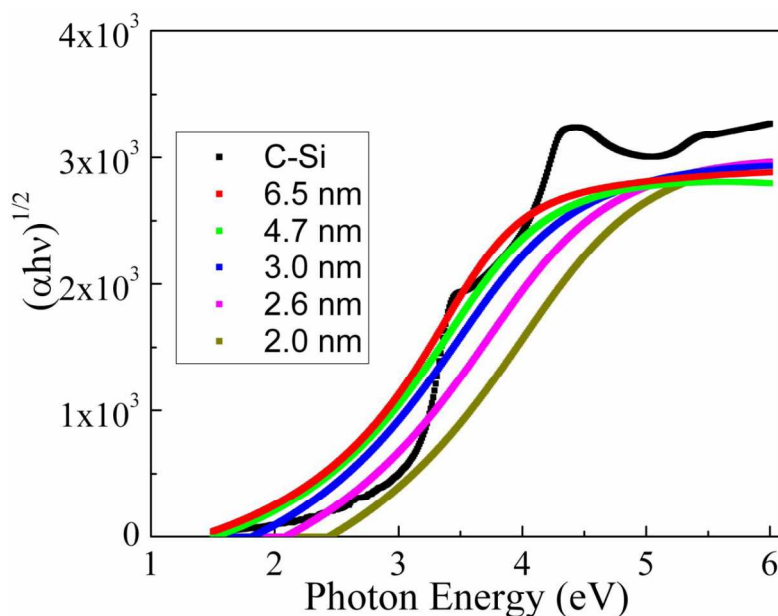


Figure 5. Plot of $(\alpha h\nu)^{1/2}$ versus photon energy ($h\nu$) for nc-Si QDs of varying sizes and bulk crystalline silicon. α denotes the absorption coefficient, calculated from $\alpha = 4\pi k/\lambda$, where k is the extinction coefficient and λ is the wavelength.

cient corresponding to the photon energy $h\nu$, extracted from the TLO fitting of the ellipsometry data. The band gap of the films, obtained by extrapolating the linear portion in Tauc's plot, varies from 1.39 to 2.45 eV.

In order to get a different perception of the optical transitions taking place and to account for the influence of size of the nc-Si QDs, the photoluminescence response of the set of samples has been obtained. The normalized PL spectra shown in Fig. 6 demonstrate a prominent blue shift in its peak energy from 1.32 to 2.13 eV, as the average size of nc-Si QDs is reduced from 6.5 to 2 nm. Qualitatively, such a trend is the most direct evidence of the quantum confinement effect occurring in nc-Si QDs embedded in a dielectric matrix e.g., a-SiO_x⁵ or a-SiN_x³⁴. In addition, the changes in the E_g values of TLO model are consistent with the shift of the peak of the PL spectra of the nc-Si QDs in a-SiO_x matrix.

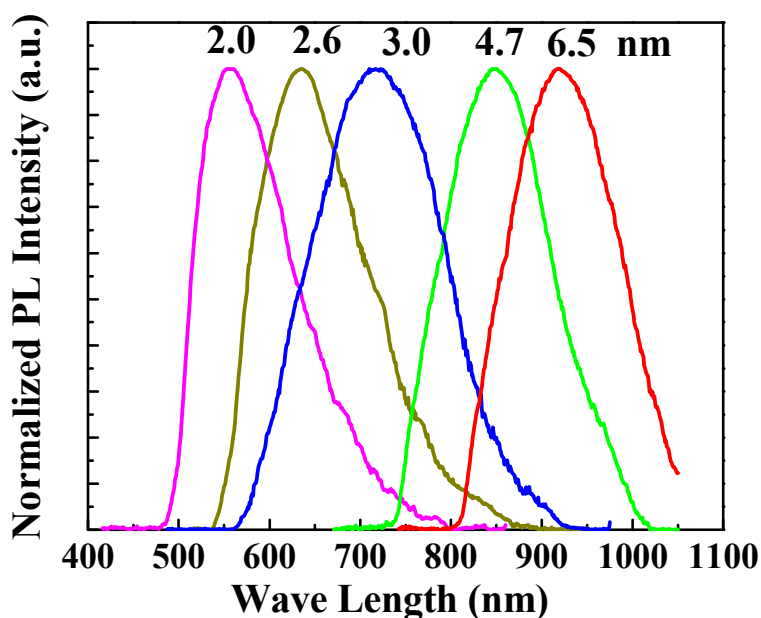


Figure 6. Normalized photoluminescence spectra of nc-Si QDs in a-SiO_x matrix with various sizes of the QDs, exhibiting blue shift of the PL peak on gradual miniaturization of the QDs.

5. Discussion:

It appears from the plot in Fig. 1 that the average size of nc-Si QDs, estimated from TEM, reduces from 6.5 to 2.0 nm while the crystalline fraction, calculated from the Raman analysis, increases from 50.2 to 63.0%, as the RF power varies from 140 to 220 W. Similar variations of the crystalline fraction in the bulk layer, from 49.1 to 68.5%, along with simultaneous lowering in its void density from ~18 to 4% has been estimated from the fitting of the ellipsometry data as presented in Table-I. While the bulk thickness remains sufficiently high, ~5,200–6,100 Å, the incubation layer systematically shrinks in thickness from ~180 to 65 Å and its void density reduces from ~26 to 14%. Similar improvement in the surface layer in terms of shrinkage in thickness from ~257 to 104 Å along with increase in crystallinity from ~34 to 52% and reduction in void density from ~29 to 15% have been extracted from the simulation of the ellipsometry data. Considering the remarkably low magnitude of the fitting parameter χ^2 , it could be inferred that the ellipsometric simulation provides a reliable comprehension on the systematic improvement of all the individual layers of the thin films comprised of nc-Si QDs embedded in a-SiO_x matrix, as a consequence of gradual increase in the applied RF power to the interacting plasma in RF glow discharge. In addition, simultaneous miniaturization of nc-Si QDs with number density in abundance, makes the material extremely suitable for devices.

The crystallization process in this He-diluted (SiH₄ +CO₂) plasma system could be typically controlled by the energy transfer to the growth-zone through the bombardment of ionized He⁺ (24 eV) and metastable He* (20 eV) from the plasma,^{35,36} which is substantially analogous with the energy transfer mechanism by atomic-H that prevails in H₂-diluted plasma.^{37,38} The formation energy of He* being lower than that of ionized He⁺, the effect of the bombardment of He* becomes more important at low RF power. In addition, excited atoms of He* arrive at the growing film surface only at thermal velocities which are much less than the impingement velocity of He⁺ ions. In comparison with the energy transferred by He⁺ this process is much softer. Strain minimization within the primarily amorphous matrix through energy transfer by de-excitation of He* at the growth zone helps forming nucleation centers. At elevated RF power, both He* and He⁺ become reactive and those are produced at larger concentrations as well. Additional energy transfer, at higher power, helps growing nucleation centers in abundance, thereby providing increasing number density of silicon nanocrystallites within the

network. As a result, the overall crystalline volume fraction in the network increases. However, the effective precursors for crystalline growth, in particular, get statistically distributed over large density of nucleation centers. Moreover, continuously increasing flux of the growth precursors at higher RF power, although ensures higher growth rate of the material, provides lesser available time for needful development of the crystallites and terminates the growth of individual crystallites before maturity. Consequently, fabrication of tiny Si-nanocrystallites in quantum dot configuration (nc-Si QDs) with diameter 2 nm, assembled in large density $2.3 \times 10^{12} \text{ cm}^{-2}$, has been made possible by controlling the RF power at 220 W, applied to the He-diluted ($\text{SiH}_4 + \text{CO}_2$) plasma.

The dielectric functions of the material are closely related to its electronic band structure which is often described by the joint density of states (JDOS). The critical points generally noticed in the spectra of the dielectric functions of the crystalline material are considered to be originated from the singularities in the JDOS.³⁹ Fig. 3 and Fig. 4 demonstrate that the dielectric functions and the optical constants of the samples with different size of nc-Si QDs exhibit a similar nature that resembles the spectral feature of amorphous silicon, both in real and imaginary parts. The size of nc-Si QDs has a significant influence on both the magnitude and shape of the spectra for the dielectric functions and the optical constants. As the QDs are reduced in size, a noticeable decrease in the intensity and blue-shift in the peak energy with respect to both C-Si and a-Si features happens to take place for both the spectra of the dielectric functions and the optical constants. Particularly looking at the ϵ_2 -spectra in Fig. 3(b), it can be noticed that for the QDs of average size ~ 6.5 nm, the peak of the ϵ_2 -spectrum lies somewhere in between the two critical points $E_1 \sim 3.4$ eV and $E_2 \sim 4.3$ eV of bulk C-Si.^{22,40,41} As the size of Si QDs is gradually reduced to ~ 2 nm, the transition energy associated with this peak systematically blue shifts and approaches towards the E_2 of C-Si. Following the systematic changes in the ϵ_2 -spectra it appears that for reducing diameter of nc-Si QDs the peak amplitude diminishes, the distribution becomes broadened and the peak position blue-shifts in energy. The diminution could be interpreted as a disappearance of the excitonic effects in the E_1 transition, the peak broadening may indicate an amplification of disorder in the Si QDs, while the blue shift of the transition energy associated with this peak towards E_2 of C-Si may be interpreted as a consequence of band gap expansion due to quantum size effects.^{22,42} Such behaviors of ϵ_2 for nc-Si QDs have been reported by other groups, both theoretically^{43,44} and experimentally^{21,22,45}.

The increase in the parameter B that generally describes the broadening of the ϵ_2 peak and is related to the disorder in the material indicates that systematic miniaturization of the nc-Si QDs induces intrinsic disorder into the system during growth, which probably accounts from the increased grain boundary defects that is intrinsic to the size reduction. The parameter A is larger for a smaller effective mass in the TL model.³¹ Hence, smaller size Si-QDs seem to possess smaller effective mass because of their associated larger magnitude of the A parameter. This could be attributed to the increased oxygenation of the a-SiO_x matrix surrounding the nc-Si QDs and the associated enhanced Si–O to Si–Si ration in the network, as the Si–Si dipoles have a larger effective mass than the Si–O dipoles. At higher applied RF power to the He-diluted SiH₄ plasma, the terminal H atoms are replaced by bridging O atoms in the Si-network and the enhanced oxide barrier at the neighboring medium around the Si nanocluster induces miniaturization of the nc-Si QDs dimension.⁶

The band gap widening and its dependence on the size of nc-Si QDs have been demonstrated by some theoretical calculations based on quantum confinement on such system and that yields a relation:^{5,46,47,48}

$$E_g(d) = E_{g0} + q/d^n \quad (7)$$

where d is the size of the nc-Si QDs in nm, $E_g(d)$ is the band gap in eV of the nc-Si QDs, E_{g0} is the band gap of bulk C-Si at room temperature. The widening of band gap estimated via the TL parameterization and PL measurements discussed above have been plotted in Fig. 7 and the best fit of those individual data to the theoretical equation above, results in two different sets of factors: $E_{g0}= 1.15$ eV, $q= 3.72$, $n=1.52$ and $E_{g0}= 1.15$ eV, $q= 3.08$, $n=1.46$ which are in adequate proximity. Thus, the band gap obtained in this work is in good agreement with the first-principle calculation of the optical gap of silicon nanocrystals based on quantum confinement,^{46,49} while the exponent (n) of the size dependence closely resembles other experimental reports.^{16,50}

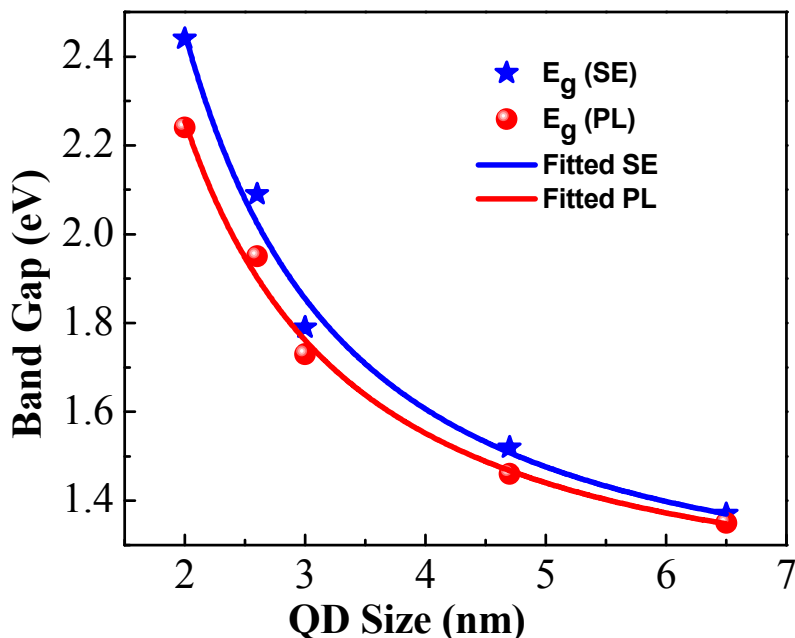


Fig. 7: Band gap expansion of the nc-Si QDs as a function of their average physical dimension.

However, the band gap obtained from the TLO fitting of the ellipsometry data is relatively high compared to the same from PL measurement, as shown in the Fig 7. This is basically due to the Stokes shift of the nc-Si QDs.⁵¹ It is more prominent in the lower size dots. Imperfect surface passivation leads to the surface defects which have relatively enhanced effect over the reduced bulk of the lower size dots, thereby more prominently hindering the effect due to quantum confinement. Ultimately, we observed a Stokes shift more vibrant in the miniaturized quantum dots. Further improvement of the material by extended passivation of the surface defects could lead to enhanced functional confinement effects for efficient optoelectronic applications of the high density tiny nc-Si QDs in devices.

Silicon nanostructures have stimulated the photonic research by its possibility of light emission with tunable energy and usable efficiency at room temperature in spite of having the indirect nature of its fundamental gap. Accordingly, it is crucial to explore the physical effects of reduced dimensionality on the electronic band structure of Si. In this study a set of samples with nc-Si QDs embedded in a-SiO_x matrix have been investigated systematically, following their changes in the absolute magnitude of the optical constants and the dielectric indices and their spectral dependence as a function of the nc-Si QD diameters between 6.5 and 2.0 nm, which turns out to be a size range where quite large changes are detected.

In order to account for the QC effect beyond the band gap in nc-Si QDs, the separation between the energies corresponding to PL peak and the absorption edge is interesting, particularly when those may vary commonly as expected from the simplest models of QC,⁵² or the PL may be much less sensitive to the QC when surface states are involved.⁵³ PL may occur due to either one of these mechanisms in some Si nanocrystals from systems of nc-Si/a-SiO_x composites.⁵⁴ Let us now discuss on the correlation between the optical band gap and the PL peak energy. There is an intensive debate both on the strong PL (in spite of the weak oscillator strength)⁵⁵ and on the unusually large Stokes shift.⁵⁶ In particular, we note that whereas a large Stokes shift was reported in many studies, only feeble shifts are realized in the present case.

Basically, three classes of thoughts are available. Firstly, it is assumed that the dissipation of the energy of the excited carriers is by optical-phonon emission, that is followed by a radiative transition of the rest of its energy.⁵⁴ Secondly, it is suggested that the radiative transition is from the band edges to a surface state at the Si/SiO₂ encapsulating shell of the crystallites.^{56,57} In the third kind, it is considered that the excitation itself causes a variation in the local configuration such that the energy allied with the transition is smaller than that associated with the absorption.^{58,59} Another school of thoughts considers a common conduction band for absorption and emission, while the radiative PL transition takes place from the conduction band to an intermediate level of valence band which is different from the level involved in the absorption processes for which there is no environmental effects.^{25,60} In addition, common conduction band energy level shifts as expected from the QC models while valence band energy level hardly varies for the shrinkage in the size of the nanocrystals. The electrons excited to the conduction band dissipate the excess energy by optical phonons that excite the vibronic Si–O surface states around the Si-ncs. This enhanced surface vibration couples with the valence band such that the Si–O configuration is changed at the surface of the Si-ncs, on the one hand, and result in the suppression of the nonradiative processes (i.e., the phonon emission) associated with the holes, on the other hand. The effect of vibronic Si–O surface states around the Si-ncs seems to be more prominent for smaller nanocrystals because of the enhanced oxide barrier, due to the inclusion of oxygen in abundance, at the neighboring a-SiO_x medium around the miniaturized nc-Si QDs dimension.⁶ The high PL intensity, the well-known sensitivity of the PL behavior to the oxidation state of the surface,⁵⁴ and the larger Stokes shift for smaller NCs are consistent with this picture.²⁵

6. Conclusion

Nanocrystalline silicon quantum dots (nc-Si QDs) of controlled sizes embedded in a-SiO_x matrix have been synthesized by spontaneous plasma processing of He-diluted (SiH₄ + CO₂) gas mixture at a low substrate temperature of 300°C, compatible for device manufacturing. Efficient energy transfer at higher power helps growing nucleation centers in abundance, thereby providing increasing number density of silicon nanocrystallites and consequently, enhanced crystalline volume fraction. Statistical distribution of the effective precursors for crystalline growth over large density of nucleation centers and simultaneous inadequate time available for the needful development of crystallites due to elevated flux of precursors, together induce termination of growth of the individual crystallites before maturity, although ensuring higher growth rate of the material. Consequently, tiny Si-nanocrystallites (~2 nm in diameter) in quantum dot configuration (nc-Si QDs) have been assembled in large density (~2.3×10¹² cm⁻²) in elevated crystalline network, which do possess promising applications in devices.

Size dependent optical constants and dielectric functions of the nc-Si QDs, including the compositional variations and thickness of different sub-layers in the thin films of nc-Si QDs embedded in a-SiO_x matrix have been obtained by proper spectroscopic simulation of the ellipsometry data in the energy range of 1.5–6.0 eV, using combination of Bruggmann effective medium approximation (BEMA) and Tauc-Lorentz oscillator dispersion model. The nc-Si QDs, in general, exhibit a significant suppression in the dielectric functions and optical constants with respect to bulk C-Si, and features a broadened peak structure analogous to that of a-Si. As the QDs are reduced in size, a gradual decrease in the intensity and blue-shift in the peak energy with respect to both C-Si and a-Si features happens to take place in case of both the spectra for the dielectric functions and the optical constants. The diminution could be interpreted as a disappearance of the excitonic effects in the E₁ transition, the peak broadening may indicate an amplification of disorder in the Si QDs, while the blue shift of the transition energy associated with this peak towards E₂ of C-Si may be interpreted as a consequence of band gap expansion due to quantum size effects. A systematic widening in the band gap of the nc-Si QDs with the reduction in its size has been identified both from TLO parameters obtained by simulation and Tauc's plot to the TLO fitted ellipsometry data, and photoluminescence measurements as well, which are in excellent agreement with the predictions of first-principles calculations based on quantum confinement.

Proper simulation of the ellipsometry data provides a reliable comprehension on the systematic changes in composition and characteristics, including the thickness, of all the individual sub-layers viz., the incubation layer, the bulk layer and the surface over-layer of the thin films, comprised of nc-Si QDs embedded in a-SiO_x matrix, grown by controlled variations of the deposition parameters. The dielectric functions of the crystalline material are closely related to the electronic band structure of the material. Ellipsometric model parameters obtained from simulation could provide explicit perception on various optical constants, e.g., refractive index, optical band gap, etc. Studies on the Stokes shift in the optical gap from the PL data could comprehend on the imperfect passivation of the surface defects on tiny nc-Si QDs. Altogether; ellipsometric simulation could enormously facilitate in the precise optimization of the deposition parameters to tune the optical and compositional characteristics of nc-Si QD thin films, suitable for specific device fabrications e.g., all-silicon tandem solar cells and light emitting diodes, using silicon nanotechnology.

Acknowledgement

The work has been done under nano-silicon projects funded by Department of Science and Technology (Nano-Mission Program) and Council of Scientific and Industrial Research, Government of India. The HRTEM studies have been performed using facilities of Unit on Nano-Science at IACS.

References:

- 1 S. Tiwari, F. Rana, H. Hanafi, A. Hartstein, E. F. Crabbé and K. Chan, *Appl. Phys. Lett.* 1996, **68**, 1377–1379.
- 2 S. K. Kim, B. H. Kim, C. H. Cho and S. J. Park, *Appl. Phys. Lett.* 2009, **94**, 183106.
- 3 S. Tiwari, F. Rana, K. Chan, L. Shi and H. Hanafi, *Appl. Phys. Lett.* 1996, **69**, 1232–1234.
- 4 X. J. Hao, A. P. Podhorodecki, Y. S. Shen, G. Zatoryb, J. Misiewicz and M. A. Green, *Nanotechnology* 2009, **20**, 485703.



- 5 D. Das and A. Samanta, *Nanotechnology* 2010, **22**, 055601.
- 6 A. Samanta and D. Das, *J. Mater. Chem.* 2011, **21**, 7452–7458.
- 7 T. W. Kim, C. H. Cho, B. H. Kim and S. J. Park, *Appl. Phys. Lett.* 2006, **88**, 123102.
- 8 L. Pavesi, L. Dal Negro, C. Mazzoleni, G. Franzo and F. Priolo, *Nature* 2000, **408**, 440–444.
- 9 R. J. Walters, G. I. Bourianoff and H. A. Atwater, *Nat. Mater.* 2005, **4**, 143–146.
- 10 G. R. Lin, C. J. Lin and C. K. Lin, *J. Appl. Phys.* 2005, **97**, 094306.
- 11 R. J. Anthony, K. Y. Cheng, Z. C. Holman, R. J. Holmes and U. R. Kortshagen, *Nano Lett.* 2012, **12**, 2822–2825.
- 12 D. Di, I. Perez-Wurfl, L. Wu, Y. Huang, A. Marconi, A. Tengattini, A. Anopchenko, L. Pavesi and G. Conibeer, *Appl. Phys. Lett.* 2011, **99**, 251113.
- 13 G. R. Lin and C. J. Lin, *Appl. Phys. Lett.* 2007, **91**, 072103.
- 14 C. H. Cheng, Y. C. Lien, C. L. Wu and G. R. Lin, *Opt. Express* 2013, **21**, 391–403.
- 15 L. W. Wang and A. Zunger, *Phys. Rev. Lett.* 1994, **73**, 1039–1042.
- 16 C. Delerue, G. Allan and M. Lannoo, *Phys. Rev. B* 1993, **48**, 11024–11036.
- 17 I. Vasiliev, S. Ogut and J. R. Chelikowsky, *Phys. Rev. Lett.* 2001, **86**, 1813–1816.
- 18 R. J. Zhang, Y. M. Chen, W. J. Lu, Q. Y. Cai, Y. X. Zheng and L. Y. Chen, *Appl. Phys. Lett.* 2009, **95**, 161109.
- 19 A. R. Feroz and I. Bloomer, *Phys. Rev. B* 1986, **34**, 7018–7026.
- 20 L. Ding, T. P. Chen, Y. Liu, C. Y. Ng and S. Fung, *Phys. Rev. B* 2005, **72**, 125419.
- 21 Z. H. Cen, T. P. Chen, L. Ding, Y. Liu, M. Yang, J. I. Wong, Z. Liu, Y. C. Liu and S. Fung, *Appl. Phys. Lett.* 2008, **93**, 023122.
- 22 Y. H. So, A. Gentle, S. Huang, G. Conibeer and M. A. Green, *J. Appl. Phys.* 2011, **109**, 064302.
- 23 D. Das, *Thin Solid Films* 2005, **476**, 237–245.



- 24 A. Hadjadj, N. Pham, P. Roca i Cabarrocas, O. Jbara and G. Djellouli, *J. Appl. Phys.* 2010, **107**, 083509.
- 25 M. I. Alonso, I. C. Marcus, M. Garriga, A. R. Goñi, J. Jedrzejewski and I. Balberg, *Phys. Rev. B* 2010, **82**, 045302.
- 26 M. Losurdo, M. M. Giangregorio, P. Capezzuto, G. Bruno, M. F. Cerqueira, E. Alves and M. Stepikhova, *Appl. Phys. Lett.* 2003, **82**, 2993–2995.
- 27 D. Das and D. Kar, *Phys. Chem. Chem. Phys.* 2014, DOI: 10.1039/C4CP03374D.
- 28 D. A. G. Bruggeman, *Annalen der Physik (Leipzig)* 1935, **24**, 636–679.
- 29 D. Das, *J. Appl. Phys.* 2003, **93**, 2528–2535.
- 30 D. Das and K. Bhattacharya, *J. Appl. Phys.* 2006, **100**, 103701.
- 31 G. E. Jellison (Jr.) and F. A. Modine, *Appl. Phys. Lett.* 1996, **69**, 371–373.
- 32 R. M. A. Azzam and N. M. Bashara, *Ellipsometry and polarized light* (North-Holland, Amsterdam), 1977, p. 153.
- 33 A. Samanta and D. Das, *Appl. Sur. Sci.*, 2012, **259**, 477–485.
- 34 B. Sain and D. Das, *Phys. Chem. Chem. Phys.* 2013, **15**, 3881–3888.
- 35 M. Jana, D. Das and A. K. Barua, *Sol. Energy Mater. Sol. Cells* 2002, **74**, 407–413.
- 36 K. Bhattacharya and D. Das, *Nanotechnology* 2007, **18**, 415704.
- 37 D. Das, *Solid State Phenom.* 1995, **44**, 227–260.
- 38 D. Das and M. Jana, *Sol. Energy Mater. Sol. Cells* 2004, **81**, 169–181.
- 39 S. Adachi, Kluwer Academic, Boston, 1999.
- 40 C. M. Herzinger, B. Johs, W. A. McGahan, J. A. Woollam and W. Paulson, *J. Appl. Phys.* 1998, **83**, 3323–3336.
- 41 A. S. Keita, A. En. Naciri, F. Delachat, M. Carrada, G. Ferblantier, A. Slaoui, *J. Appl. Phys.* 2010, **107**, 093516.
- 42 D. Amans, S. Callard, A. Gagnaire, J. Joseph, G. Ledoux and F. Huisken, *J. Appl. Phys.* 2003, **93**, 4173–4179.



- 43 H. C. Weissker, J. Furthmuller and F. Bechstedt, *Phys. Rev. B* 2004, **69**, 155310.
- 44 C. Delerue, M. Lannoo and G. Allan, *Phys. Rev. B* 2003, **68**, 115411.
- 45 D. Barba, C. Dahmoune, F. Martin and G. G. Ross, *J. Appl. Phys.* 2009, **105**, 013521.
- 46 L. W. Wang and A. Zunger, *J. Phys. Chem.* 1994, **98**, 2158–2165.
- 47 D. Das, *Solid State Commun.* 1998, **108**, 983–987.
- 48 B. Sain and D. Das, *J. Lumin.* 2015, **158**, 11–18.
- 49 S. Ogut, J. R. Chelikowsky and S. G. Louie, *Phys. Rev. Lett.* 1997, **79**, 1770–1773.
- 50 C. L. Wu and G. R. Lin, *AIP Advances* 2012, **2**, 042162.
- 51 R. Q. Zhang, A. D. Sarkar, T. A. Niehaus and T. Frauenheim, *Phys. Stat. Sol. B* 2012, **249**, 401–412.
- 52 A. Saar, *J. Nanophotonics* 2009, **3**, 032501.
- 53 M. V. Wolkin, J. Jorne, P. M. Fauchet, G. Allan and C. Delerue, *Phys. Rev. Lett.* 1999, **82**, 197–200.
- 54 S. Godefroo, M. Hayne, M. Jivanescu, A. Stesmans, M. Zacharias, O. I. Lebedev, G. Van Tendeloo and V. V. Moshchalkov, *Nat. Nanotechnol.* 2008, **3**, 174–178.
- 55 D. Kovalev, H. Heckler, G. Polisski, J. Diener and F. Koch, *Opt. Mater.* 2001, **17**, 35–40.
- 56 Y. Kanemitsu and S. Okamoto, *Phys. Rev. B* 1998, **58**, 9652–9655.
- 57 K. Murayama, H. Komatsu, S. Miyazaki and M. Hirose, *J. Non-Cryst. Solids* 1996, **198-200**, 953–956.
- 58 E. Degoli, G. Cantele, E. Luppi, R. Magri, D. Ninno, O. Bisi and S. Ossicini, *Phys. Rev. B* 2004, **69**, 155411.
- 59 L. Pan, Z. Sun and C. Sun, *Scr. Mater.* 2009, **60**, 1105–1108.
- 60 X. L. Wu, S. J. Xiong, D. L. Fan, Y. Gu, X. M. Bao, G. G. Siu and M. J. Stokes, *Phys. Rev. B* 2000, **62**, R7759–R7762.



Graphical Abstract

Energy blue shift due to quantum confinement effects in tiny nc-Si QDs accompanied by larger Stokes shifts in PL at smaller dimensions.

